PHYSICAL REVIEW A **85**, 013829 (2012)

Bragg wave coupling in self-assembled opal photonic crystals

Rajesh V. Nair[*] and B. N. Jagatap
Atomic and Molecular Physics Division, Bhabha Atomic Research Centre, Mumbai, India 400 085

(Received 12 April 2011; published 23 January 2012)

The optical properties of three-dimensionally-ordered self-assembled photonic crystals are studied in the Bragg wave coupling regime. Angle-resolved photonic stop gap measurements show the Bragg wave coupling extending over an angular range of 18°. The new diffraction peak originating at the Bragg wave coupling regime is due to the $(\bar{1}11)$ stop gap. The Bragg wave coupling regime is analyzed for photonic crystals with different lattice constants and refractive index contrasts. For lower-index-contrast photonic crystals, Bragg wave coupling occurs at a lower angle of incidence as compared to higher-index-contrast photonic crystals of similar lattice constants. The exchange of energy between the diffraction peaks in the coupling regime is discussed. Experimental results are compared with theoretical calculations and they are in good agreement. Furthermore, we demonstrate tunable stop gap with high reflectance and photonic strength in the fiber-optic communication wavelength range.

DOI: 10.1103/PhysRevA.85.013829 PACS number(s): 42.70.Qs, 42.25.Fx, 41.20.Jb

I. INTRODUCTION

Recently, much effort has been made to fabricate and study the science of a class of nanophotonic structures called photonic crystals. Photonic crystals have a periodically varying dielectric constant along three orthogonal directions with a period of the order of the wavelength of light [1–3]. They can tailor the light propagation and emission [4,5] and also offer the opportunity to trap photons in very small volumes at intentionally made point defects [6]. Due to the periodic nature of the structure, photon dispersion relations are organized into bands similar to electron bands in semiconductors. This results in a frequency range called "photonic stop gap" where the propagation of light is forbidden. When the photonic stop gaps along different directions overlap in frequency, for each polarization state of the incident light, a photonic band gap is formed. In the frequency range of photonic band gap, the density of states (DOS) goes to zero which results in an ultimate control of the light propagation and emission [3,4,7]. A sought-after goal in nanophotonics research is to demonstrate a photonic band gap requiring certain crystal symmetries and index contrast [8]. Recently, a signature of the photonic band gap has been demonstrated through a systematic study of reflectivity spectra along different crystal directions and light polarizations on a diamondlike inverse woodpile silicon photonic crystal [9]. On the other side, low-refractive-index-contrast photonic crystals such as colloidal photonic crystals, which do not exhibit photonic band gap, have also received considerable attention [3,4,10–12]. The colloidal photonic crystal is an ideal platform to study the physics of light-matter interaction associated with light propagation in periodic structures [10–12].

Self-assembled colloidal photonic crystals often result in the face centered cubic (fcc) crystal form with the (111) plane parallel to the substrate [13–16]. Most of the optical studies documented in literature are from the (111) plane and in the low-energy region [3,13,15–18]. There exist few works in the literature that study the light-matter interaction in the high-energy side of the photonic stop gap [19–24]. The difficulty in observing the higher-order stop gaps is due to the increased unwanted light scattering in the high-energy region and it is a subject of considerable debate recently [25,26]. Another remarkable physical phenomenon, which is seldom observed in photonic crystals, is the Bragg wave coupling, i.e., the coupling between the Bragg waves diffracted from two or more crystal planes at certain conditions of the incident wave vector. While Bragg wave coupling is well known for x-rays in crystals [27], it is rarely observed in photonic crystals. This is due to the fact that photonic crystals are artificially made crystals and therefore may have many unwanted defects and disorder which hamper the observation of Bragg wave coupling. Another important aspect is the finite size effects in the synthesized samples. Physical phenomena demonstrated theoretically rely on the assumption that the unit cell in the crystals is extended to infinity in all three orthogonal directions. The pertinent question is when a real synthesized photonic crystal behaves similarly to an infinitely long crystal so as to eliminate the finite size effects. In the synthesized photonic crystals, finite size effects can be eliminated with samples having thickness larger than the Bragg length.

The coupling of light diffracted by different crystal planes in the depth of the crystal is required to observe the Bragg wave coupling. Photonic stop gap observed at near-normal incidence from the (111) plane shows a single diffraction peak [23]. This is the first-order stop gap along the [111] direction or in Γ-L direction in reciprocal space. This process involves two coupled waves; the incident and the diffracted. When Bragg wave coupling occurs, it is no longer a two-wave coupled phenomenon since there are other Bragg diffracted waves from different crystal planes with different Miller indices. This results in diffraction spectra that are complex and are very difficult to observe experimentally. The observation of Bragg wave coupling assumes importance as it is the basis of photonic band gap which is the overlap between the diffraction spectra along different crystal symmetry directions [9].

Bragg wave coupling is little analyzed in literature and its demonstration is limited to the visible wavelength range [21,28–34]. This may be due to the fact that it is easier to synthesize self-assembled photonic crystals with stop gap in the visible wavelength region as compared to those in the

---

[*] rvnair@barc.gov.in

near-infrared wavelength ranges [14]. Adding to this is the difficulty in synthesizing self-assembled photonic crystals of superior optical quality in the near-infrared wavelength region as the size of the building blocks (polymer beads) becomes larger, i.e., of the order of 800 nm [14]. It is extremely difficult to synthesize photonic crystals of superior optical quality using larger spheres due to the reduced Brownian motion in the colloidal suspension and large polydispersity of the spheres [3]. However, by carefully tuning the fabrication conditions, high-quality photonic crystals can be fabricated in the near-infrared wavelength region.

In the present work, we report angle-resolved mapping of photonic stop gaps in self-assembled opal photonic crystals with different lattice constants and index contrasts. At near-normal incidence of light we measure ten diffraction peaks and to the best of our knowledge this is the highest number ever observed. We show the evolution of Bragg wave coupling regime in photonic crystals for a large range of incident angles. Bragg wave coupling extends over an angular range of 18° in the present work. The multiple Bragg peaks are coupled and they have the same peak reflectance. Our theoretical calculation of Bragg wave coupling regime is in good agreement with the experimental results. Theoretical and experimental results show that the incident angle at which Bragg wave coupling occurs is dependent on the index contrast of the photonic crystals for similar lattice constants and symmetry. We discuss here the exchange of energy between the diffraction peaks in the regime of Bragg wave coupling. Our opal photonic crystals are thick (Bragg length is smaller than the thickness of the sample) and hence result in an extremely well-resolved Bragg wave coupling regime with high reflectance. While our focus is on the optical communication wavelength ranges owing to its technological relevance, we also discuss the coupling regime in the visible wavelength ranges. We believe such a detailed experimental observation and quantitative analysis of Bragg wave coupling is not yet reported.

The paper is organized as follows. The experimental details of the photonic crystal fabrication using the self-assembling method are briefly explained in Sec. II. Results and analysis of the optical characterization of the photonic crystals are presented in Sec. III. Angle-resolved mapping of photonic stop gap and Bragg wave coupling are explained here. Section IV provides a detailed discussion on the Bragg wave coupling in photonic crystals with different lattice constants and refractive index contrasts, and its comparison with theoretical calculations. Important conclusions arising from this work are given in Sec. V.

II. EXPERIMENTAL DETAILS

We use the convective self-assembly of colloidal suspensions for the fabrication of photonic crystals in the visible and near-infrared wavelength ranges [13]. Commercially available colloidal suspensions are used for the fabrication (M/s Microparticles, GmbH). We use polystyrene (PS) spheres of diameter $D = 803 \pm 26$ nm, 266 ± 6 nm, and polymethyl methacrylate (PMMA) spheres of diameter $D = 287 \pm 8$ nm. The diameters are as specified by the manufacturer. Details of the fabrication procedure are explained elsewhere [13,17] and briefly sketched here. We use 1 wt% of the colloidal suspension in a cuvette with a clean glass slide placed in the suspension. The whole assembly is kept in a controlled temperature oven at 55 °C for PS spheres ($D = 803 \pm 26$ nm), and 45 °C for PS spheres ($D = 266 \pm 6$ nm) and PMMA spheres ($D = 287 \pm 8$ nm), respectively. The high temperature used for the fabrication with PS spheres of $D = 803 \pm 26$ nm is to compensate for the reduced Brownian motion of the colloidal particles [14]. Typical time taken for the sample growth is ~4 days. The samples are post-annealed at 75 °C for 2 h to increase the mechanical stability. Structural quality of the photonic crystals is analyzed using field emission scanning electron microscopy (FESEM). The samples are silver coated prior to the FESEM characterization. Optical characterizations of the photonic crystals are done using a PerkinElmer LAMBDA-950 spectrophotometer with a halogen lamp as the light source and beam dimensions of 5 mm × 5 mm. The light beam used is unpolarized.

III. RESULTS AND ANALYSIS

The FESEM image of the synthesized photonic crystals with sphere diameter of 803 nm is given in Fig. 1. The image is taken around a vertical crack, which is intrinsic to the self-assembling method, to show good ordering on the top surface as well as in the depth of the photonic crystals. The top surface of the image confirms the hexagonal packing of spheres representing the (111) planes in the fcc lattice. These (111) planes are parallel to the substrate. Figure 1(a) shows a large surface area view of a self-assembled PS photonic crystal of sphere diameter 803 nm. The vertical crack that separates the crystal surface into domains is clearly observed. A closer view into the depth of the crack, on both sides of the domain, is shown in the left and right insets in Fig. 1(a). Identical orientation of spheres (hexagonal packing in the depth) on both sides of the crack shows the mirror-symmetric nature of domains within the photonic crystal structure which are due to the twinned nature of fcc domains. The twinned fcc domains have paramount importance in the Bragg wave coupling, to be discussed in Sec. IV. The cross-sectional image in Fig. 1(b) shows the $(\bar{1}11)$-type planes in the fcc lattice inclined to the top (111) plane. A white patch seen around the spheres is due to charging effects. A part of the fcc Brillouin zone with high-symmetry points relevant to our experiment is schematically inscribed in Fig. 1(b). Photonic stop gap is probed along the L point (normal incidence) and the incident light direction is changed so as to probe the stop gaps along the L-K-L_1 trajectory on the surface of the fcc Brillouin zone [red dashed line in Fig. 1(b)]. This is discussed in detail in the following sections.

The signature of the photonic stop gap is observed through the reflectivity and transmittance measurements. At stop gap wavelength, high reflectivity of light is accompanied by low transmission of light through the structure resulting in vanishing of DOS for those light modes [23]. The photonic crystal structure behaves like a photonic insulator at the stop gap wavelength. The photonic stop gap measured from the (111) plane of the photonic crystal is given in Fig. 2(a) for near-normal incidence of light. A peak in reflectivity spectra ~1750 nm ($a/\lambda_c = 0.65$, a is the fcc lattice constant, λ_c is

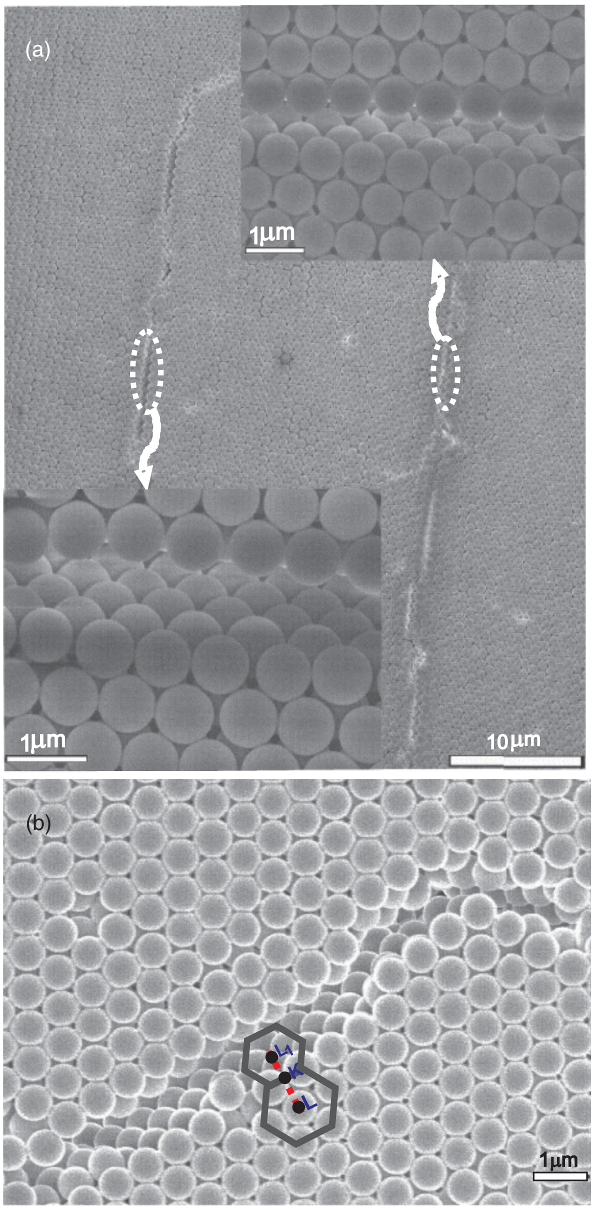

FIG. 1. (Color online) (a) A large area view of the photonic crystal surface indicates the presence of cracks that separate the crystal surface into domains. The left and right insets represent the ordering in the depth of the crack on either side of the domain. The identical orientation of spheres in the depth of the sample on either side of the domain shows the mirror-symmetric nature due to twinned fcc domains. (b) Top surface of the sample represents (111) plane and the cross-sectional image reveals ($\bar{1}11$)-type plane of fcc lattice. A section of the fcc Brillouin zone with relevant high-symmetry points is shown. The red dashed line indicates the measurement trajectory. White patches seen around spheres are due to charging effects.

the stop gap wavelength) with a peak reflectance of 57% is accompanied by a trough in transmittance spectra with a low transmittance of 18%. This is the signature of the photonic stop gap. On either side of the stop gap, the structure behaves like a homogeneous medium. The experimentally observed stop gap frequency of $a/\lambda_c = 0.65$ agrees well with the photonic band structure calculation [21].

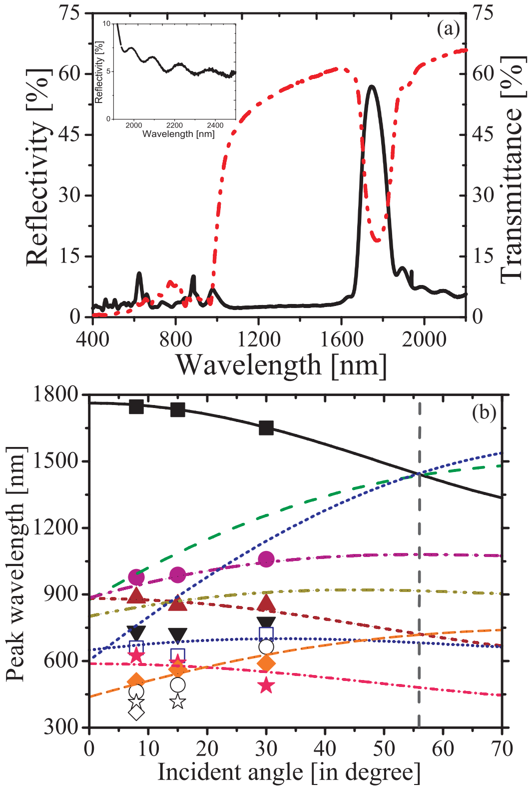

FIG. 2. (Color online) (a) Reflectivity (black solid line) and transmittance (red dash-dot line) for a photonic crystal composed of PS spheres of effective diameter 750 nm showing stop gap at 1750 nm. The peak in the reflectivity spectra agrees with the trough in the transmission spectra which is the signature of photonic stop gap. Higher-order reflectivity peaks are visible in the wavelength ranges between 400 and 1000 nm. Inset shows the Fabry-Perot oscillations on the long-wavelength side of stop gap. (b) Calculated Bragg wavelength for different crystal planes as a function of external angle of incidence of light. Symbols shows peak reflectance wavelength obtained from measured reflectivity spectra at 8°, 15°, and 30° angles of incidence. Lines represent the calculated Bragg wavelengths for different crystal planes, such as (111) plane (black solid line), (200) plane (green dashed line), ($\bar{1}11$) plane (blue dotted line), (220) plane (magenta dash-dot line), (311) plane (dark yellow dash-dot-dot line), (222) plane (brown short dashed line), (331) plane (dark blue short-dot line), (400) plane (orange broken line), and (333) plane (pink short-dash-dot line). The vertical dashed line indicates crossing of bands at 55° incidence.

The photonic strength or the ratio between the full width at half maximum ($\Delta\lambda$) and the stop gap wavelength (λ_c) is measured to be 6.57%. From the band structure calculations [21,35], the photonic strength estimated for self-assembled PS photonic crystals is 6.50%. This close agreement between the experimental and estimated photonic strengths shows the superior optical quality of our photonic crystals which is necessary to observe Bragg wave coupling. The Bragg length (L_B), i.e., the distance through which light propagates at stop gap wavelength in photonic crystals before being completely attenuated can be calculated using the formula [35] $L_B = 2d_{hkl}/\pi S$, where d_{hkl} is the distance between the crystal planes in the [hkl] direction and S is the photonic strength. The measured L_B along the [111] direction is 6 μm or $10d_{111}$. The Fabry-Perot (FP) oscillations [see inset in Fig. 2(a)] observed on either side of the stop gap indicate uniform thickness of the sample and also good ordering of each layer in the depth of the photonic crystal. The thickness (t) of the photonic crystal is estimated from the FP fringes using the formula [36], $t = 1239/(2n_{\mathrm{eff}}\Delta E)$, where n_{eff} is the effective refractive index and ΔE (in eV) is the difference in energy positions of two consecutive troughs in the FP oscillations. In the long-wavelength side of the stop gap, we estimate $t \approx 14$ μm (~22 ordered layers) $\approx 2.4L_B$, which indicates that the finite size effects are eliminated in our photonic crystals. These large numbers of ordered layers in the crystal have major implications in the Bragg wave coupling. The reflectivity and transmittance spectra are very complex in the wavelength range between 400 and 1000 nm in Fig. 2(a). This wavelength range, where second-, third-, and other higher-order reflectivity peaks originate, is the high-energy optical response of the photonic crystals [23].

Angle-resolved reflectivity spectra provide information about photonic stop gaps at different angles of incidence. In Fig. 2(b), we show the measured peak reflectivity wavelengths (symbols) for three different incident angles together with the calculated wavelength of peak reflectivity from different crystal planes in the fcc lattice using the relation [31]

$$\lambda_{hkl} = 2n_{\mathrm{eff}}d_{hkl}\cos\left[\alpha - \sin^{-1}\left(\frac{1}{n_{\mathrm{eff}}}\sin\theta\right)\right], \qquad (1)$$

where λ_{hkl} is the Bragg wavelength diffracted from the crystal plane with Miller indices (hkl), d_{hkl} is the distance between the (hkl) crystal planes, α is the angle between the (hkl) plane and the (111) plane, and θ is the external angle of incidence of light. The calculations are done using an effective sphere diameter (D_{eff}) of 750 nm which is obtained by fitting the experimentally measured stop gap wavelength from the (111) plane with Eq. (1) for $\theta < 45°$. Note here that D_{eff} is somewhat less than that (803 ± 26 nm) specified by the manufacturer. In all further analysis we use the sphere diameter of 750 nm (D_{eff}), $d_{111} = 0.816D_{\mathrm{eff}}$, and $n_{\mathrm{eff}} = 1.44$ for PS photonic crystals. The (hkl) planes used in the calculations in Fig. 2(b) are (111) plane (black solid line), (222) plane (brown short dashed line), (333) plane (pink short-dash-dot line), (200) plane (green dashed line), (220) plane (magenta dash-dot line), (331) plane (dark blue short-dot line), (400) plane (orange broken line), and ($\bar{1}11$) plane (blue dotted line). The (111) stop gap wavelength (black closed squares) agrees well with calculated stop gap wavelength (black solid line). The reflectivity peak at 980 nm (magenta closed circles) matches with those calculated for (220) stop gap wavelength (magenta dash-dot line). At this wavelength ($a/\lambda_c = 1.1$), light can also couple to flat bands resulting in a high-reflectivity peak and enhanced DOS [20,22,23]. The second-order stop gap at 890 nm (brown upward triangles) agrees well with calculated (222) stop gap wavelengths (brown short dashed line). The reflectivity peak at 624 nm (pink closed stars) is the third-order stop gap which agrees with calculated (333) stop gap wavelengths (pink short-dash-dot line). The reflectivity peak at 671 nm (dark blue open squares) is in agreement with calculated (331) stop gap wavelengths (dark blue short-dot line). The reflectivity peaks at 510 nm (orange closed diamonds) matches with calculated (400) stop gap wavelengths (orange broken line). Some of the other reflectivity peaks do not have agreement with calculated bands. This may be due to the fact that a reflectivity peak can also be caused by light coupling to flat bands as there are many flat bands present in the investigated wavelength range [20,22]. At near-normal incidence ($\theta \approx 8°$), we have observed ten diffraction peaks which to the best of our knowledge is the highest number ever observed. It is interesting to notice the diffraction curves belonging to the (111), (200), and ($\bar{1}11$) planes cross each other around $\theta \approx 55°$ (indicated by a vertical dashed line). We will focus on this band crossing in more detail in what follows.

An angle-resolved photonic stop gap is shown in Figs. 3(a)–3(c). With increase in θ on the (111) plane, the photonic stop gap shifts towards the lower-wavelength region. For $\theta < 45°$, the peak reflectance and width of the (111) stop gap are hardly changed at all as shown in Fig. 3(a). However, for $\theta > 45°$ the situation changes drastically such that the peak reflectance of the (111) stop gap reduces and a new reflectivity peak appears at the low-wavelength band edge. Starting at $\theta = 47°$ [green dotted line in Fig. 3(a)], a new reflectivity peak becomes more intensified and it shifts towards the higher-wavelength side of the (111) stop gap with further increase in angle of incidence. The peak reflectance of the (111) stop gap reduces continuously whereas the peak reflectance of the new reflectivity peak increases. At $\theta = 50°$ [black solid line in Fig. 3(b)], the new reflectivity peak is more resolved and the strength of the (111) reflectivity peak reduces marginally. At this angle of incidence, the new reflectivity peak is well resolved and the original (111) stop gap starts to split. At $\theta = 53°$ [red dotted line in Fig. 3(b)], two reflectivity peaks are equally separated. They have the same peak reflectance values and same width. The two reflectivity peaks are marked with vertical dashed lines in Fig. 3(b). At this angle of incidence two Bragg waves are simultaneously excited in the crystal with the same scattering strengths and therefore they repel each other with equal reflected intensity. This is the avoided crossing region at which Bragg wave coupling takes place. The two Bragg diffracted waves are separated by 100 nm and they are coupled [28]. At $\theta = 56°$, the strength of the (111) peak starts to increase, peak reflectance of new diffraction peak starts to decrease, and both peaks shift in opposite directions. It is interesting to see that the diffraction spectra at 50° and 56° are symmetric. The avoided crossing region which results in the repulsion of two stop gaps takes place between $\theta = 50°$ and 56°. With further increase in θ, the new reflectivity peak moves towards the higher-wavelength side whereas the (111) reflectivity peak shifts towards the lower-wavelength side, as is seen in Fig. 3(c). Also the peak reflectance of the (111) peak starts to increase whereas the peak reflectance of the new reflectivity peak starts to decrease. This shows that the energy is continuously exchanged between these two reflectivity peaks from the moment the new reflectivity peak starts to appear at $\theta = 47°$. The equal exchange of energy occurs at the avoided crossing region.

An important aspect observed in Fig. 3 is the reduction in peak reflectance of the (111) diffraction peak. A small percentage (~5%) change in peak reflectance value of the (111) diffraction peak is generally observed for off-normal

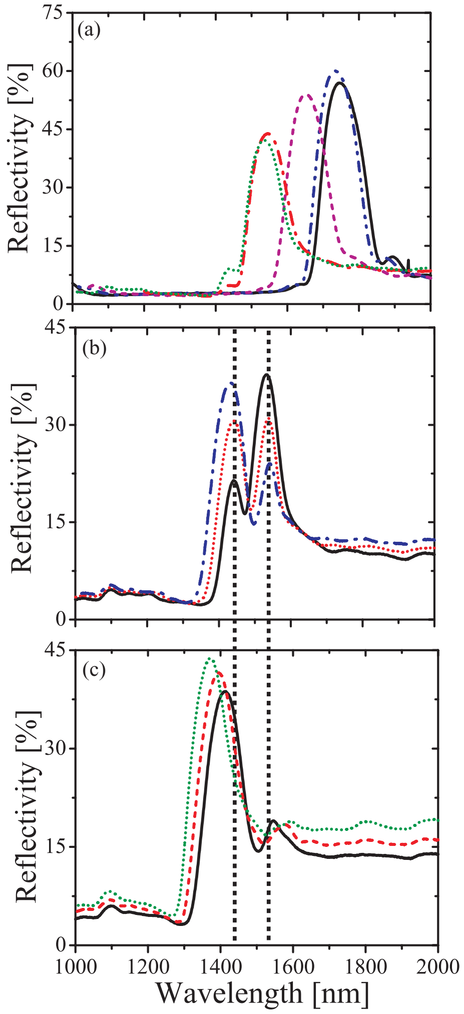

FIG. 3. (Color online) (a) Photonic stop gap at angles of incidence of 8° (black solid line), 15° (blue dash-dot-dot line), 30° (magenta dashed line), 45° (red dash-dot line), and 47° (green dotted line). With increase in angle of incidence, stop gap shifts towards shorter wavelengths. At angles of incidence of 45° and 47°, a new reflectivity peak starts appearing near the low-wavelength edge of the stop gap. (b) Photonic stop gap at angles of incidence of 50° (black solid line), 53° (red dotted line), and at 56° (blue dash-dot line). At 53° incidence, the two diffraction peaks are well separated and have equal reflected intensity. The peak wavelengths are indicated by vertical dashed lines. (c) Photonic stop gap at angles of incidence of 59° (black solid line), 62° (red dashed line), and at 65° (green dotted line). Both diffraction peaks are shifts in opposite directions.

incidence of light. In contrast the peak reflectance value in Fig. 3(a) shows drastic reductions beyond $\theta = 45^\circ$. The peak reflectance values of the two diffraction peaks for $\theta \geqslant 45^\circ$ are depicted in Fig. 4. Here we observe that with increase in θ (up to 55°), the peak reflectance value of the (111) diffraction peak (closed circles) decreases whereas that for the new diffraction peak (open circles) increases. This clearly shows that the energy is being continuously transferred to new diffraction peak from the (111) diffraction peak. When these diffracted waves are crossed around $\theta \approx 55^\circ$, they have the same peak reflectance as the energy is equally shared between them. For $\theta > 55^\circ$, peak reflectance of the (111) peak increases whereas the peak reflectance of the new diffraction peak decreases. This shows the energy is now transferred from the new diffraction peak back to the original (111) diffraction peak. The sum of the peak reflectance of these two diffraction peaks (marked by triangles) is also given in Fig. 4. It is seen that this sum is nearly constant in the Bragg wave coupling regime and its value is equal to reflectance at near-normal incidence (∼60%, dashed line in Fig. 4). This confirms our hypothesis that the energy is being continuously exchanged between the (111) diffraction peak and the new diffraction peak. The constancy of the peak reflectance sum also indicates that energy is not lost due to any unwanted scattering inside the sample or on the surface.

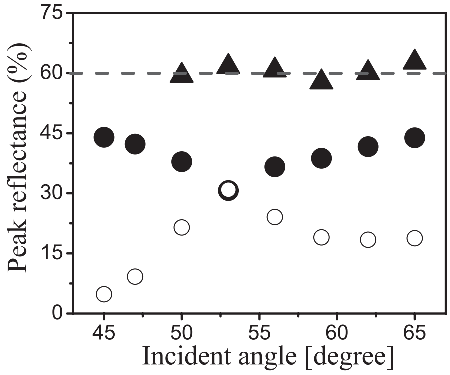

FIG. 4. Peak reflectance value of the (111) diffraction peaks (closed circles), new diffraction peaks (open circles), and their sum (triangles) as a function of angle of incidence of light in the Bragg wave coupling regime. Initially the peak reflectance of the (111) stop gap decreases and that for the new diffraction peak increases with increase in angle of incidence and they equalize when the Bragg wave coupling occurs. The peak reflectance of the (111) diffraction peak increases and that for the new diffraction peak decreases with further increase in angle of incidence. The sum of reflectance of both peaks is equal to the reflectance at near-normal incidence (dashed line).

A simple schematic illustration of Bragg wave coupling regime in reciprocal space is given in Fig. 5(a). A cross section of the fcc Brillouin zone is given with relevant high-symmetry points Γ, L, U, X, K, and L_1. The incident wave vector is $\vec{k}_0$. The two diffracted wave vector from the (111) and $(\bar{1}11)$ planes are represented by $\vec{k}_1$ and $\vec{k}_2$, respectively. The reciprocal lattice vectors along the Γ-L and Γ-L_1 direction are denoted by $\vec{G}_{111}$ and $\vec{G}_{\bar{1}11}$, respectively. For near-normal incidence of light, the diffraction condition is satisfied for only the (111) plane; i.e., $\vec{k}_0 + \vec{G}_{111} = \vec{k}_1$. This is a two-wave coupled process as there are only the incident and diffracted waves along the Γ-L direction. When the incident wave vector $\vec{k}_0$ passes through the K point, two diffraction conditions are satisfied simultaneously for the (111) and $(\bar{1}11)$ planes, namely, $\vec{k}_0 + \vec{G}_{111} = \vec{k}_1$ and $\vec{k}_0 + \vec{G}_{\bar{1}11} = \vec{k}_2$ as shown in Fig. 5(a). For an incident wave vector along the K point, the scattered wave vectors $\vec{k}_1$ and $\vec{k}_2$ are simultaneously generated. This is a three-wave coupled process involving $\vec{k}_0$, $\vec{k}_1$, and $\vec{k}_2$, which represents the Bragg wave coupling regime. A similar kind of Bragg wave coupling is also possible along the Γ-X direction.

The diffraction process can be visualized as follows: When θ crosses 45°, light diffracted by the crystal planes in the

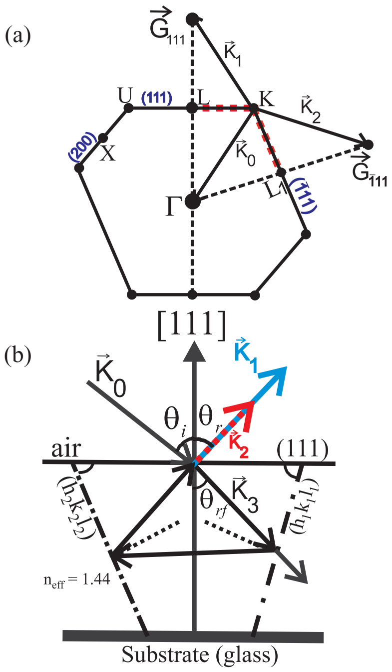

FIG. 5. (Color online) (a) A simple schematic illustration of the Bragg wave coupling regime is represented using a cross section of the fcc Brillouin zone. The high-symmetry points (Γ, L, U, X, K, and L_1) relevant to our experiment are shown. Here $\vec{k}_0$ represents the incident wave vector; $\vec{k}_1$,$\vec{k}_2$ are diffracted wave vectors from (111) and ($\bar{1}11$) planes, respectively. The incident wave vector $\vec{k}_0$ along the K point gives the Bragg wave coupling process with two reciprocal lattice vectors $\vec{G}_{111}$ and $\vec{G}_{\bar{1}11}$. The red dashed line shows the trajectory relevant to our experiment. (b) The Bragg wave coupling scheme in real space. The incident wave vector $\vec{k}_0$ at an angle θ_i onto the (111) plane of photonic crystal, generates reflected wave vector $\vec{k}_1$ (blue solid arrow) and transmitted wave vector $\vec{k}_3$. The transmitted wave is diffracted by the crystal plane $(h_1k_1l_1)$, propagates through the crystal, and can be in resonance with another plane $(h_2k_2l_2)$, wherein it gets diffracted again to propagate in parallel with $\vec{k}_1$ and is detected in specular reflection geometry as $\vec{k}_2$ (red dashed arrow). The $(h_2k_2l_2)$ is the mirror-symmetric plane of $(h_1k_1l_1)$ due to the twinned nature of fcc domains. Equal reflectance intensity occurs when all the diffraction processes are in resonance with each other.

depth of the photonic crystal is re-directed to other crystal planes which re-diffract the light along the specular direction together with the (111) diffraction peak. At a specific angle of incidence, the diffraction strength of both the peaks is equal. In Fig. 5(b) we have shown a possible physical mechanism in real space wherein the Bragg wave coupling occurs. The incident wave vector $\vec{k}_0$ at an angle of incidence of θ_i on the (111) plane generates a diffracted wave vector $\vec{k}_1$ from the (111) plane and a transmitted wave vector $\vec{k}_3$. The angle θ_i is chosen to be 53°, which is the angle at which two diffraction peaks have equal intensity in our experiment, and θ_rf is ~33.7°. The transmitted wave can be in resonance with the $(h_1k_1l_1)$ plane and it generates another diffracted beam which propagates through the photonic crystal. This beam can again be re-diffracted by another $(h_2k_2l_2)$ plane with wave vector $\vec{k}_2$ (red dashed arrow), propagate collinearly with $\vec{k}_1$ (blue solid arrow), and get detected in the specular reflection geometry. The $(h_2k_2l_2)$ is a mirror-symmetric plane of $(h_1k_1l_1)$ due to the twinned nature of fcc domains, to be discussed later. In this way wave vectors $\vec{k}_1$ and $\vec{k}_2$ are parallel to each other. The coupling between $\vec{k}_1$ and $\vec{k}_2$ is maximal when the diffraction from the $(h_1k_1l_1)$ plane of the photonic crystal is efficient. In our case this happens at an angle of incidence of 53° which results in equal diffracted intensity for the two diffraction peaks. This can happen only when the samples have extremely good ordering in the depth of the photonic crystals, otherwise the diffracted beam by the $(h_1k_1l_1)$ plane would fade away due to unwanted scattering by defects and result in vanishing of the Bragg wave coupling, or it may be less pronounced. The Bragg wave coupling observed in the present case over an angular range of 18° indicates the finest ordering present in our samples. In Fig. 4 we explain how the energy of two diffracted beams exchanges between them and show that the total energy remains constant. Here in Fig. 5(b), we show the different diffraction processes; their coupling takes place inside the photonic crystals. The two diffracted beams are constantly exchanging the energy between them. The peak wavelength depends on the angle of incidence of light and that signifies that the observed phenomena are from the depth of the crystal and not due to any surface effects of three-dimensional photonic crystals. The challenge is now to find the crystal planes that are responsible for the new diffraction peak, which will be explained in the following section.

IV. DISCUSSION

With increase in external angle of incidence, the (111) diffraction peak shifts towards the lower-wavelength side whereas the new diffraction peak shifts towards the higher-wavelength side. In Fig. 6(a) we show the evolution of the (111) stop gap (closed symbols) and the new diffraction peak (open symbols) for a PS photonic crystal of $D_\text{eff} = 750$ nm. The stop gap wavelengths are extracted through Gaussian fittings of measured reflectivity spectra. The Bragg wavelengths for three important planes in the fcc Brillouin zone, namely, (111) (black solid line), (200) (blue dashed line), and ($\bar{1}11$) (red dotted line) calculated using Eq. (1) are also given in Fig. 6(a). It is interesting to see the crossing of (200), ($\bar{1}11$) stop gap wavelength with (111) stop gap wavelength at around $\theta \approx 55°$ (shown with a vertical blue dashed line). Because of the crossing of these bands, for $\theta \approx 55°$, the (111) stop gap intercepts the new diffraction peak and they shift in opposite directions with further increase in θ. This trend is also evident in calculated Bragg wavelengths. Furthermore, our experimental results are in good agreement with the calculated stop gap crossing. When the external angle of incidence increases, the internal angle of incidence for two planes responsible for the diffraction peak increases for the (111) stop gap while it decreases for the new diffraction peak and both peaks shift in opposite direction. Both peaks in the crossing region are well resolved with equal intensity and separated with a clear trough in between them [see Fig. 3(b)]. This is due to large number of ordered layers with less defects and disorder. It is very important to note that in our photonic crystals the finite size effects are eliminated as $t \approx 2.4\ L_\text{B}$ and therefore Bragg wave coupling shows extremely well-resolved diffraction peaks with high reflectance. It should also be noted

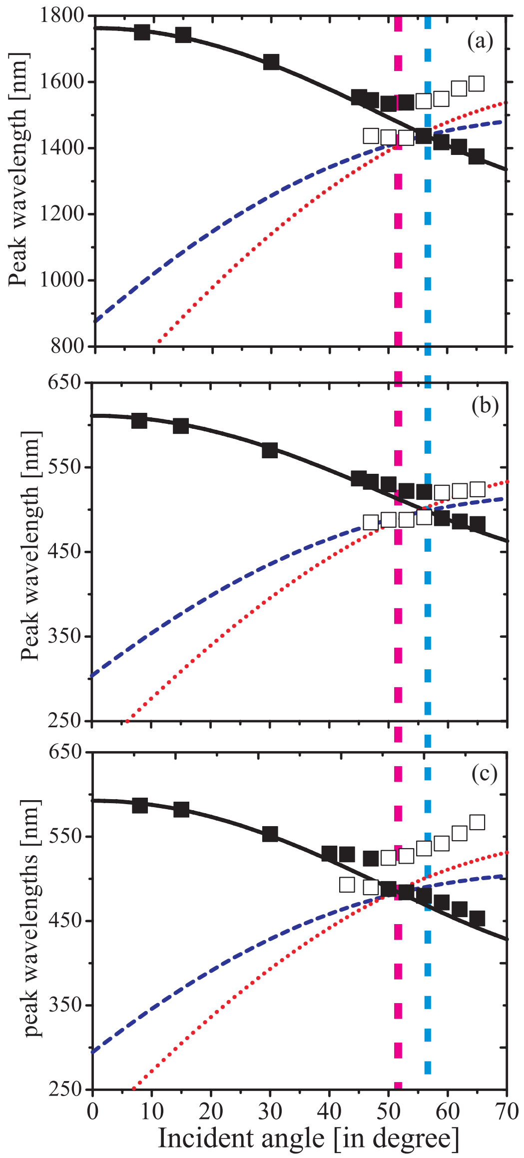

FIG. 6. (Color online) (a), (b) Calculated stop gap wavelength for three different crystal planes in the fcc Brillouin zone, namely, (111) (black solid line), (200) (blue dashed line), and $(\bar{1}11)$ (red dotted line) along with experimental stop gap wavelengths (symbols) as a function of angle of incidence for PS photonic crystal with $D_{\text{eff}} = 750$ nm and $D_{\text{eff}} = 260$ nm, respectively. The closed and open symbols represents the measured (111) and $(\bar{1}11)$ stop gaps, respectively. Bragg wave coupling occurs at an angle of incidence of 55° indicated with a vertical blue dashed line in both (a) and (b). Bragg wave coupling occurs at different wavelengths in (a) and (b) because of the difference in lattice constant even though the refractive-index contrast is the same. (c) Calculated stop gap wavelength for three different crystal planes in fcc Brillouin zone, i.e., (111) (black solid line), (200) (blue dashed line), and $(\bar{1}11)$ (red dotted line) along with experimental stop gap wavelengths as a function of angle of incidence for PMMA photonic crystal with $D_{\text{eff}} = 267$ nm. The closed and open symbols represent measured (111) and $(\bar{1}11)$ stop gaps, respectively. Bragg wave coupling occurs at an angle of incidence of 50° indicated with a vertical pink dashed line. Due to reduction in index contrast, Bragg wave coupling occurs at lower angle of incidence in (c) as compared to (a) and (b).

that the (200), $(\bar{1}11)$ stop gap wavelength crosses the (111) stop gap at the same external angles of incidence. This is due to the fact that the length LU or LK on the face of the fcc Brillouin zone are identical [31]. This makes it difficult to assign the new diffraction peak to the correct crystal plane. The evidence of the correct diffraction plane becomes clearer only when the incident wave vector crosses the U or K point on the surface of thefcc Brillouin zone. When the incident wave vector crosses the U point towards the X point, then the (200)-type planes will be responsible for Bragg wave coupling, or if the incident wave vector crosses the K point towards the L_1 point, then the $(\bar{1}11)$-type planes will be responsible for Bragg wave coupling as seen in Fig. 5(a). The FESEM image (see Fig. 1) taken from the cross sections of the domain which is probed during the optical characterization shows the $(\bar{1}11)$-type planes inclined to the top (111) planes. The case is the same for adjacent domains of the sample. This shows that as the angle of incidence increases to larger values, $(\bar{1}11)$-type planes may contribute to Bragg wave coupling in the present case. We also observe that some domains have square packing in the top few layers representative of (200)-type planes but, in the depth, we find hexagonal packing of spheres representative of $(\bar{1}11)$-type planes. Since the structural imaging is only a visualization tool, the planes responsible for the new diffraction peak must be assigned through optical spectroscopy. Also it is the reflectivity peak wavelength that decides the diffraction process as it originates from the depth of the photonic crystal to build up the Bragg diffraction. Therefore the plane responsible for the new diffraction peak is assigned through reflectivity measurements. We observe in Fig. 6(a) that, beyond the crossing angle, the new diffraction peak (open symbols) is in better agreement with the $(\bar{1}11)$ dispersion curve (red dotted line) as compared to the (200) dispersion curve (blue dashed line). Therefore we conclude that the new diffraction peak in the Bragg wave coupling regime is from the $(\bar{1}11)$-type planes in the depth of the photonic crystals. We also compare our experimentally observed reflectivity peak wavelengths to the calculated photonic band structure reported in the literature on similar photonic crystal structures [22,31]. The reflectivity peak appears near the crossing point at a reduced frequency of $a/\lambda_c = 0.73$. The reduced frequency obtained from calculated photonic band structure is at $a/\lambda_c = 0.75$ for a wave vector near the K point [22,31]. This also indicates that the Bragg wave coupling occurs at the K point with the incident wave vector moving towards the K point, and the wave vector trajectory is Γ-L-K-L_1 in the fcc Brillouin zone [see red dashed line in Fig. 5(a)]. In Ref. [30], Baryshev *et al.* also address the new diffraction peak in the crossing region as being due to the $(\bar{1}11)$-type planes for a self-assembled silica photonic crystal. They find that the measured peak reflectivity wavelength is in agreement with the $(\bar{1}11)$ dispersion curve for an angle of 61.2° between the (111) and $(\bar{1}11)$ planes. The decrease in angle between the planes from the ideal case (70.5°) is attributed to the anisotropy in the sample growth in addition to the limited number of ordered layers. But in our case the measured peak reflectivity wavelengths are in close agreement with the $(\bar{1}11)$ dispersion curve calculated for an ideal fcc lattice with an angle of 70.5° between the (111) and $(\bar{1}11)$ planes.

In order to corroborate our results we conducted experiments with a self-assembled PS photonic crystal with D_{eff} of 260 nm (obtained from the Bragg's law fit to the stop gap wavelengths for $\theta < 45^\circ$). This gives us a stop gap in the visible region at a wavelength (λ_c) of 605 nm and $a/\lambda_c = 0.61$, which agrees with Γ-L stop gap frequency from the calculated photonic band structure [21]. Photonic strength is estimated to be 6.60% and L_B is 2 μm or $10d_{111}$. The thickness (t) of the photonic crystal estimated from the FP fringes in the long-wavelength side of the stop gap is 8.6 μm ($\sim$40 ordered layers) and $t \sim 4.3\, L_B$. Angle-resolved mapping of the photonic stop gap reveals Bragg wave coupling at an external angle of incidence of 55°. The experimental results are similar to those shown for the near-infrared wavelength region (see Fig. 3). The experimentally observed stop gap wavelengths together with the calculated stop gap wavelengths for the (111), (200), and $(\bar{1}11)$ planes are given in Fig. 6(b). The closed and open symbols represents the (111) and $(\bar{1}11)$ stop gaps at different θ. Bragg wave coupling occurs at $\theta = 55^\circ$ (shown by a vertical blue dashed line) with a well-resolved Bragg diffraction peak having equal reflectance. The measured $(\bar{1}11)$ stop gaps (open symbols) are in good agreement with the calculated $(\bar{1}11)$ dispersion (red dotted line) curve as seen in Fig. 6(b). It is also very clear that the band crossing takes place exactly at the same θ in both Figs. 6(a) and 6(b). The wavelength region where the Bragg wave coupling occurs is around 500 nm in Fig. 6(b) as compared to those at 1500 nm in Fig. 6(a). This is due to the difference in lattice constants even though the index contrast is the same. Thus the wavelength region of avoided crossing is proportional to the lattice constant. This is another confirmation that the basis of observed phenomena is Bragg diffraction. Thus we have conclusively shown the Bragg wave coupling in the near-infrared and visible wavelength region for photonic crystals with different lattice constants.

We have performed Bragg wave coupling experiments on self-assembled PMMA photonic crystals of an effective sphere diameter $D_{\mathrm{eff}} = 267$ nm (obtained from the Bragg's law fit to the stop gap wavelengths at angles below 45°) to demonstrate our results for low-refractive-index-contrast photonic crystals. The photonic stop gap is centered at a wavelength (λ_c) of 587 nm with a photonic strength of 6.30% and L_B is 2.2 μm or $10d_{111}$. The thickness of the photonic crystal estimated from the FP fringes is 7.6 μm ($\sim$35 ordered layers) and $t \approx 3.4\, L_B$, thereby indicating that the finite size effects are removed. The angle-resolved photonic stop gap wavelengths are shown in Fig. 6(c) in the same perspective as in Figs. 6(a) and 6(b). We experimentally measure the Bragg wave coupling similar to PS photonic crystals. We observe very well-resolved multiple diffraction peaks having similar reflectance but with one exception, that the band crossing takes place around $\theta \approx 50^\circ$ indicated using a vertical pink dashed line in Fig. 6(c). Our experimental results clearly show the Bragg wave coupling at $\theta = 50^\circ$, the angle at which the band crossing takes place. Similar to the case of PS photonic crystals, here also the new diffraction peak is addressed as the stop gap from the $(\bar{1}11)$ plane. The refractive index contrast of the PMMA photonic crystal is low which results in the crossing of dispersion curves at lower angles of incidence as compared to high-index-contrast PS photonic crystals. These experimental results demonstrate well-resolved Bragg wave coupling for lower-index-contrast photonic crystals and that shows this phenomenon is dependent on the ordering of the crystal planes and not on the refractive index contrast. Thus even for small-refractive-index-contrast photonic crystals with well-ordered crystal planes and $t > L_B$, well-resolved Bragg wave coupling must be seen.

The measured peak reflectivity wavelengths are in good agreement with the calculated $(\bar{1}11)$ dispersion curve as evident in Figs. 6(a)–6(c). The calculated dispersion curve shows crossing of stop gaps at $\theta \approx 55^\circ$ and at $\theta \approx 50^\circ$ for PS and PMMA photonic crystals, respectively. This crossing is also in good agreement with measured peak reflectivity wavelengths. This clear agreement is due to the large number of ordered layers with fewer defects and disorder in the depth of the photonic crystals together with $t > L_B$. The thickness of the samples strongly affects the optical properties of photonic crystals in the Bragg wave coupling regime. A closer look into Figs. 6(a) and 6(b) for PS photonic crystals indicate that as the (111) stop gap (closed symbols) approaches the band crossing region at $\theta \approx 55^\circ$, it deviates from the (111) dispersion curve (black solid line) and moves apart when it intercepts the $(\bar{1}11)$ stop gap (open symbols) at the crossing angle. Beyond the crossing angle, the (111) stop gap continues to follow its dispersion curve. This clearly demonstrates that (111) stop gap repulsion takes place in the Bragg wave coupling regime. Similar behavior is also seen in Fig. 6(c) for PMMA photonic crystals at $\theta \approx 50^\circ$.

In Fig. 7, we illustrate the reflectivity spectra measured at "+"θ and "–"θ along the $L \rightarrow U$ (K) directions for a PS photonic crystal with $D_{\mathrm{eff}} = 750$ nm. The closed symbols represent the $+\theta$ direction and open symbols represents the $-\theta$ direction. The spectra measured at $\pm\theta$ are well overlapped with each other at different values of θ. This shows that the planes in the depth of the crystal are mirror symmetric to each other due to the twinning nature of the fcc domain in the samples. The perfect overlapping of reflectivity spectra shows identical orientations of crystal domains in the samples. In addition to optical spectroscopy, the FESEM image [see Fig. 1(a)] mapped around a crack (which separates the crystal domains) indicates hexagonal packing of spheres in the depth of photonic crystal structure which is representative of $(\bar{1}11)$-type planes. The orientation of spheres in the depth of the sample is identical on either side of the domain as seen in Fig. 1(a). This confirms that the domains are separated from each other with $(\bar{1}11)$-type planes inclined to top (111) planes and hence the new peak appearing in the angle-resolved spectra measured at "+"θ and "–"θ is from the $(\bar{1}11)$ planes. Our analysis also follows the interpretation given in Ref. [30] as twinning and exchange of energy between diffraction peaks plays a vital role in the Bragg wave coupling process.

Another experimental procedure that may help to assign the new peak in the reflectivity spectra in the coupling regime to the respective crystal plane is polarization dependent angle-resolved transmittance or reflectivity measurement. When a transverse magnetic (TM) polarized wave is incident on a photonic crystal at the Brewster angle (55° in our case) with respect to the respective planes, then the reflectivity peak for that particular plane will be absent and that for the other

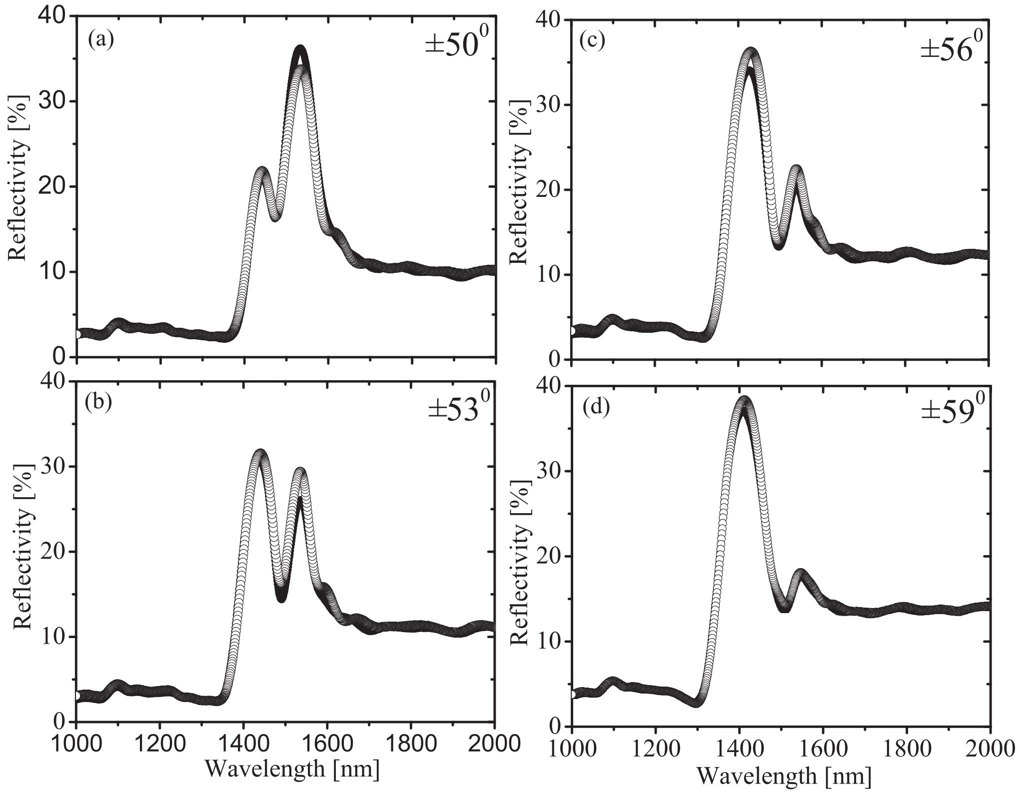

FIG. 7. (a)–(d) Angle-resolved reflectivity spectra at $+\theta$ (closed symbols) and at $-\theta$ (open symbols) along $L \rightarrow U$ (K) direction of fcc Brillouin zone. The respective measurement angles are shown in each figure. The reflectivity spectra are very well overlapped with each other in both $+\theta$ and $-\theta$ measurements. The similarity in reflectivity spectra at $+\theta$ and $-\theta$ indicates that the photonic crystal structure has twinned fcc domains. Note the very good overlapping in terms of peak reflectance, stop gap wavelength, and width, which indicates fine structural ordering preserved in the depth of the photonic crystals and identical orientation of fcc domains.

crystal plane will be detected in reflection or in transmittance measurements. Rigorous theoretical calculations in terms of band structure or the reflectivity spectra at the Bragg wave coupling regime in photonic crystals are necessary in this context, which are however, beyond the scope of the present work. Very good optical quality of our photonic crystals with $t > L_B$ shows Bragg wave coupling for an angular range of 18°. Also, in the coupling regime, stop gap wavelengths are nearly the same due to the flattening of photonic bands [28]. This can result in nearly the same suppression in DOS at those wavelengths.

Recent research shows that the Bragg wave coupling regime can significantly enhance the Faraday rotation in magnetophotonic crystals [37]. This indicates the possibility of using Bragg wave coupling demonstrated in the present work for device applications in the optical communication wavelength region. Moreover, Fig. 3(a) shows the tuning of the stop gap with high reflectance value in the wavelength region of fiber-optic communication. The experimentally measured photonic strength is in good agreement with the photonic band structure. Thus high-quality photonic crystals with very good stop gap properties are realized in our work at the telecommunication wavelength region. Polystyrene being a third-order nonlinear optical material [11], where the refractive index can be changed extremely fast using Kerr effect, ultrafast switching of the stop gap is feasible in the telecommunication wavelength range using photonic crystals described in the presented work. Experiments in this regards are currently being initiated.

V. CONCLUSIONS

In summary, we have shown a systematic study of Bragg wave coupling in photonic crystals in the visible and near-infrared wavelength ranges. Our results reveal well-resolved multiple Bragg peaks with equal reflected intensity in the band crossing region. The Bragg wave coupling regime extends over 18° of angle of incidence with well-resolved Bragg peaks. The experimental results are in good agreement with the calculated dispersion curves. The calculated crossing of stop gaps is also demonstrated through reflectivity measurements. We have discussed the reduction in the peak reflectance value of the stop gap, in the regime of Bragg wave coupling, in terms of the exchange of energy between the Bragg peaks. Our analysis shows that the new diffraction peak observed in the reflectivity spectra in the Bragg wave coupling regime is due to the $(\bar{1}11)$ plane and incident wave vector shifts towards the K point in the Γ-L-K-L_1 trajectory on the fcc Brillouin zone. The experimental results and calculated dispersion curves shows that with reduction in refractive-index contrast the Bragg wave coupling occurs at lower angles of incidence. In addition to Bragg wave coupling, we have demonstrated tunable stop gaps with high reflectance and photonic strength in the wavelength region of interest in fiber-optic communication.

ACKNOWLEDGMENTS

The authors thank Professor R. Vijaya, IIT Bombay, for providing the colloidal suspensions used in the present work and Professor S. S. Major, IIT Bombay, for the use of the spectrophotometer. R.V.N. thanks the Board of Research in Nuclear Science (BRNS), DAE, Government of India for Dr. K. S. Krishnan Research Fellowship.

---

[1] E. Yablonovitch, Phys. Rev. Lett. **58**, 2059 (1987).
[2] S. John, Phys. Rev. Lett. **58**, 2486 (1987).
[3] C. Lopez, Adv. Mater. **15**, 1679 (2003).
[4] P. Lodahl, A. F. van Driel, I. Nikolaev, A. Irman, K. Overgaag, D. Vanmaekelbergh, and W. L. Vos, Nature **430**, 654 (2004).
[5] J. D. Joannopoulos, P. R. Villeneuve, and S. Fan, Nature **386**, 143 (1997).
[6] K. J. Vahala, Nature **424**, 839 (2003).
[7] S. Ogawa, M. Imada, S. Yoshimoto, M. Okano, and S. Noda, Science **305**, 227 (2004).
[8] M. Maldovan and E. L. Thomas, Nat. Mater. **3**, 593 (2004).
[9] S. R. Huisman, R. V. Nair, L. A. Woldering, M. D. Leistikow, A. P. Mosk, and W. L. Vos, Phys. Rev. B **83**, 205313 (2011).
[10] M. Maymo, J. Martorell, A. Molinos-Gomez, and F. Lopez-Calahorra, Opt. Express **14**, 2864 (2006).
[11] P. P. Markowicz, H. Tiryaki, H. Pudavar, P. N. Prasad, N. N. Lepeshkin, and R. W. Boyd, Phys. Rev. Lett. **92**, 083903 (2004).
[12] R. V. Nair, R. Vijaya, K. Kuroda, and K. Sakoda, J. Appl. Phys. **102**, 123106 (2007).
[13] P. Jiang, J. F. Bertone, K. S. Hwang, and V. L. Colvin, Chem. Mater. **11** 2132 (1999).
[14] D. J. Norris, E. G. Arlinghaus, L. Meng, R. Heiny, and L. E. Scriven, Adv. Mater. **16**, 1393 (2004).
[15] I. I. Tarhan and G. H. Watson, Phys. Rev. Lett. **76**, 315 (1996).
[16] H. Miguez, F. Meseguer, C. Lopez, A. Mifsud, J. S. Moya, and L. Vazquez, Langmuir **13**, 6009 (1997).
[17] R. V. Nair and R. Vijaya, J. Phys. D: Appl. Phys. **40**, 990 (2007).
[18] R. V. Nair and R. Vijaya, Appl. Phys. A **90**, 559 (2008).
[19] H. Miguez, V. Kitaev, and G. A. Ozin, Appl. Phys. Lett. **84**, 1239 (2004).
[20] J. F. Galisteo-Lopez and C. Lopez, Phys. Rev. B **70**, 035108 (2004).
[21] J. F. Galisteo-Lopez, E. Palacios-Lidon, E. Castillo-Martinez, and C. Lopez, Phys. Rev. B **68** 115109 (2003).
[22] E. Pavarini, L. C. Andreani, C. Soci, M. Galli, F. Marabelli, and D. Comoretto, Phys. Rev. B **72**, 045102 (2005).
[23] R. V. Nair and R. Vijaya, Phys. Rev. A **76**, 053805 (2007).
[24] L. A. Dorado, R. A. Depine, and H. Míguez, Phys. Rev. B **75**, 241101(R) (2007).
[25] L. A. Dorado, R. A. Depine, and H. Míguez, Phys. Rev. A **78**, 037801 (2008).
[26] R. V. Nair and R. Vijaya, Phys. Rev. A **78**, 037802 (2008).
[27] S.-L. Chang, *X-Ray Multiple-Wave Diffraction* (Springer-Verlag, Berlin, 2004).
[28] H. M. van Driel and W. L. Vos, Phys. Rev. B **62**, 9872 (2000).
[29] S. G. Romanov, T. Maka, C. M. Sotomayor Torres, M. Muller, R. Zentel, D. Cassagne, J. Manzanares-Martinez, and C. Jouanin, Phys. Rev. E **63**, 056603 (2001).
[30] A. V. Baryshev, A. B. Khanikaev, R. Fujikawa, H. Uchida, and M. Inoue, Phys. Rev. B **76**, 014305 (2007).
[31] L. C. Andreani, A. Balestreri, J. F. Galisteo-López, M. Galli, M. Patrini, E. Descrovi, A. Chiodoni, F. Giorgis, L. Pallavidino, and F. Geobaldo, Phys. Rev. B **78**, 205304 (2008).
[32] S. Schutzmann, I. Venditti, P. Prosposito, M. Casalboni, and M. V. Russo, Opt. Express **16**, 897 (2008).
[33] A. Tikhonov, J. Bohn, and S. A. Asher, Phys. Rev. B **80**, 235125 (2009).
[34] R. V. Nair and R. Vijaya, Appl. Opt. **48**, G59 (2009).
[35] L. Bechger, P. Lodahl, and W. L. Vos, J. Phys. Chem. B **109**, 9980 (2005).
[36] S. G. Romanov, M. Bardosova, D. E. Whitehead, I. M. Povey, M. Pemble, and C. M. Sotomayor Torres, Appl. Phys. Lett. **90**, 133101 (2007).
[37] S. Baek, A. V. Baryshev, and M. Inoue, Appl. Phys. Lett. **98**, 101111 (2011).